Modelling adhesive contact problems involving a layered elastic solid and cylindrical indenter using Lennard Jones potential

W. W. F. Chong[a,c] and S. J. Chidlow[b,1]

[a] *National Centre for Advanced Tribology (nCATS), Faculty of Engineering and the Environment, University of Southampton, UK*

[b] *Department of Mechanical Engineering and Mathematical Sciences, Oxford Brookes University, UK*

[c] *Faculty of Engineering and the Environment, University of Southampton Malaysia Campus (USMC), Nusajaya, Johor, Malaysia*

Abstract

This paper presents an iterative algorithm that solves for the displacement and sub-surface stresses induced within a layered elastic solid adhering to a rigid cylindrical indenter under lightly loaded conditions. The solid is assumed to comprise a functionally graded coating of finite thickness bonded to a homogeneous substrate of infinite extent and is assumed to be in a state of plane strain which allows a two-dimensional analysis to be performed. The Lennard-Jones potential is used to model the adhesive force acting between the indenter and solid whilst the effects of surface adhesion are characterised using Tabor's parameter.

A selection of numerical results for the adhesive contact problem are presented which indicate that the maximum pressure and induced sub-surface stresses increase dramatically as Tabor's parameter increases. It is also found that the shear modulus and thickness of the coating have a significant effect on material behaviour with harder coatings experiencing significantly larger tensile stresses but smaller surface displacement than softer coatings. The present investigation allows us to deduce that at smaller scales, surface adhesion can be instrumental in causing wear or potential material failure if

[1] *w.chong@soton.ac.uk, sj.chidlow@brookes.ac.uk*

coatings are improperly designed.

Keywords: Lennard-Jones potential, layered solids, contact mechanics, surface adhesion, sub-surface stress fields

---

1. Introduction

Functionally graded materials (FGMs) are increasingly being used as protective coatings within engineering applications. Potential areas of use for such materials include magnetic storage media, nano and microelectromechanical systems, barrier coatings for structural components, dental implants and articulating surfaces in hip and knee prostheses [1]. Graded materials are designed so that their physical and mechanical properties vary continuously or discretely throughout their depth [1]. As a result, these materials can be used to redistribute thermal stresses [2] and reduce stress concentrations which can help minimise the local driving force for crack growth [3] and lead to an increased susceptibility to damage through wear.

The ability to accurately determine the likely effects of using different graded elastic coating types is crucial and many mathematical models have been developed to investigate the effects of material property gradients on resistance to normal loading, sliding, rolling and fretting contact and wear. The contact problem of a rigid body indenting a homogeneously elastic solid was initially solved by Hertz [4] who provided analytical solutions for the two and three dimensional case. However, FGMs are not homogeneous and cannot be accurately modeled using Hertzian theory. By assuming that modulus of elasticity within a functionally graded material follows either a power law or exponential variation, Giannakopoulos and Suresh [5] proposed simple analytical models to determine the displacements and stresses within a three-dimensional graded elastic medium. Wang *et al* [6] applied the Fast Fourier Transform (FFT) method to investigate partial-slip contacts involving graded materials within a three-dimensional context.

The full three-dimensional contact problem involving FGMs is complicated and it is often very difficult, if not impossible to solve such problems analytically. A useful simplification that is often adopted is to assume that the FGM is in a state of plane strain which allows a two-dimensional analysis to be performed. In this context, Guler and Erdogan [7] used Fourier transform techniques to solve the contact problem for a graded elastic layered solid. The authors assume that the coated system can be modeled as

an FGM of finite thickness perfectly bonded to a homogeneously elastic substrate and allow for an exponential variation of the shear modulus within the FGM. Ke and Wang [8] proposed a similar model to Guler and Erdogan but model the FGM as a series of sub-layers in which the shear modulus varies linearly. Teodorescu and Rahnejat [9] solved the contact problem involving an inhomogeneous material comprising two distinct yet homogeneous layers using Fourier series decomposition for an automotive cam/tappet contact. More recently, Chidlow *et al* [10] proposed solutions for the displacements and stresses within a graded elastic layered solid in terms of a Fourier series which are analytic if the applied pressure is known exactly. As in the work of Guler and Erdogan [7], the shear modulus within the coating is assumed to vary exponentially but the presented model is devised in a generic form for ease of adapting it to engineering applications ranging from nano to macro scale.

One of the problems that occurs when attempting to model contact problems on a small scale is that adhesion between two contacting surfaces becomes significant due to short-ranged intermolecular forces acting between nano and micro-sized colloidal particles [11, 12]. The classical Hertzian model does not allow for this behaviour and thus alternate models have been sought to accurately describe this phenomenon. An early investigation into this subject was conducted by Boussinesq [13] who found that unlike the pressure distribution obtained by Hertz for homogenous solids, the pressure distribution over a circular contact region became infinite along the edge of the contact. This led to Bradley [14] proposing a contact model between rigid spheres brought into contact solely due to surface forces (e.g. van der Waals force). Hamaker [15] refined Bradley's work, leading to the introduction of Hamaker's constant which is used to determine Van der Waals force. However, neither of the aforementioned approaches allowed for particle deformation which limits the usage of these methods. To overcome this deficiency, Derjaguin [16] included contact deformations of particles while investigating the influence of short-range intermolecular forces.

Perhaps the best known models of surface adhesion in a three-dimensional context were proposed by Johnson *et al* [17] and Derjaguin *et al* [18]. Johnson *et al* [17] suggested that surface adhesion occurs only within the contact with infinitely large tensile stresses occurring along the edges of the contact, leading to the development of the JKR adhesion model. Derjaguin *et al* [18] however hypothesised that adhesion occurs only outside of the contact so that Hertzian theory can be applied within the contact region. This model

is referred to as the DMT model.

It has been observed that the JKR model accurately describes the behaviour of soft, compliant materials with a high surface energy whilst the DMT model corresponds well to hard materials with a low surface energy [19]. These provided mathematical models at two distinct ends of the material spectrum. In order to approximate contact behaviour using the appropriate model, Tabor's parameter (denoted μ), was introduced as a measure for the magnitude of elastic deformation as compared to the range of surface forces [20]. To describe the transition from the DMT model to the JKR model, Muller *et al* [21] presented a self-consistent numerical analysis using the Lennard-Jones potential for contacting spheres with evenly distributed intermolecular forces in an elastic half-space. Whilst this model does link together the JKR and DMT models, it was not discussed in sufficient detail to allow other authors to replicate their solutions. The idea of a transitional region however was later described by Maugis [22] using the Dugdale potential. This model compliments the work of Johnson *et al* [17] and Derjaguin *et al* [18] by describing the transition from JKR to DMT-like behaviour.

Maugis' adhesion model utilises a square-well like Dugdale potential. However, contact solutions based on realistic force laws have been proven to contribute more reliable knowledge to the understanding of the contact behaviour between deformable bodies under the influence of surface forces (e.g. surface adhesion [23]). For homogeneous materials, Attard and Parker [24] used the Lennard-Jones potential to show a non-monotonic trend of the pull-off force against Tabor's parameter for a rigid spherical indenter pressed against a homogeneous solid. In a later iteration, Feng investigated the contact behaviour of spherical elastic particles using an adhesive model based on the Lennard-Jones potential [23]. Wu [25], adapted the approach by Feng to [23], simulate the adhesive contact between a cylinder and a half-space. He compared simulated results to those obtained using the modified Maugis' model for a line contact, initially introduced by Leng *et al* [26] and fully evaluated by Johnson and Greenwood [27].

The majority of research conducted on adhesive behaviour has focussed solely on homogeneously elastic materials but some attempts have been made to extend such investigations to inhomogeneous elastic materials. Using the surface force apparatus, McGuiggan *et al* [28] found that the pull-off force for a layered solid could vary significantly from that predicted by the JKR model. For functionally graded materials in a layered solid configuration, Mary *et al* [29] proposed a semi-analytical model that describes the adhesive contact

between layered solids and axisymmetric probes. Johnson and Sridhar [30] also presented an adhesive model, based on the original JKR model, for a layered solid with a homogeneous elastic coating. Lately, Chidlow *et al* [31] investigated the effects of surface adhesion between a rigid cylindrical indenter and a layered solid when in contact using Maugis's Dugdale model.

This study proposes a new model for the adhesive line contact between a two-dimensional layered elastic solid and rigid cylindrical indenter. The solid is deemed to comprise of a graded elastic coating bonded to a homogeneous substrate whilst the adhesion between surfaces is modeled using the Lennard-Jones potential. A selection of numerical results are presented within this work that aim to determine the effects of adhesion on the surface displacement and sub-surface stresses induced within a lightly loaded contact during the pre and initial contact region. To the best of the author's belief, the model proposed within this work is the only one currently available that attempts to characterise the adhesive behaviour of FGMs using Lennard Jones potential.

2. Mathematical Model

We consider the adhesive contact between a layered elastic solid in a state of plane strain and a rigid cylindrical indenter as illustrated in figure 1.

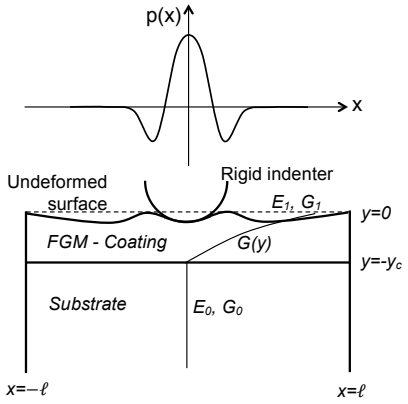

Figure 1: Lennard-Jones adhesive contact between a rigid cylindrical indenter and a layered solid comprising a functionally graded coating and homogeneous substrate

The solid occupies the semi-infinite region $-\infty < y \leq 0, -l \leq x \leq l$ and is split into distinct layers that represent a graded elastic coating of thickness

y_c and a homogeneous substrate of infinite extent. The inhomogeneity of the coating is assumed to depend exponentially on the vertical co-ordinate so that the shear modulus of the solid is defined as

$$G(y) = \begin{cases} G_1 e^{\zeta y}, & -y_c \leq y \leq 0, \\ G_0, & -\infty < y < -y_c \end{cases} . \tag{1}$$

The parameter ζ is chosen to ensure that the shear modulus is continuous at $y = -y_c$ and is defined as

$$\zeta = \frac{1}{y_c} \ln\left(\frac{G_1}{G_0}\right). \tag{2}$$

Under the assumption that the coating and substrate are perfectly bonded and that contact between the solid and indenter is frictionless so that the boundary conditions

$$\sigma_{yy} = -p(x), \tag{3}$$
$$\sigma_{xy} = 0 \tag{4}$$

hold on the solid surface $y = 0$, we can use the model of Chidlow et al. [10] to describe the displacement and stresses induced within the layered solid. This model gives the horizontal displacement $u(x, y)$ and vertical displacement $v(x, y)$ within each region as

$$u^{(c)}(x,y) = \sum_{n=1}^{\infty} \xi_n^T(y)\Omega_n \begin{pmatrix} \frac{(1-2\nu)P_n}{2G_0} \\ 0 \end{pmatrix} \cos\left(\frac{1}{2}\beta_n(x+l)\right), \tag{5}$$

$$v^{(c)}(x,y) = -\sum_{n=1}^{\infty} \xi_n^T(y)\Gamma_n\Omega_n \begin{pmatrix} \frac{(1-2\nu)P_n}{2G_0} \\ 0 \end{pmatrix} \sin\left(\frac{1}{2}\beta_n(x+l)\right) \tag{6}$$

which holds for $-y_c \leq y \leq 0$, and

$$u^{(s)}(x,y) = \sum_{n=1}^{\infty} \frac{e^{\frac{1}{2}\beta_n(y+h)}}{\delta_n} \psi^T(y)\Psi_n \begin{pmatrix} \frac{(1-2\nu)P_n}{2G_0} \\ 0 \end{pmatrix} \cos\left(\frac{1}{2}\beta_n(x+l)\right), \tag{7}$$

$$v^{(s)}(x,y) = \sum_{n=1}^{\infty} \frac{e^{\frac{1}{2}\beta_n(y+h)}}{\delta_n} \psi^T(y)\Phi_n\Psi_n \begin{pmatrix} \frac{(1-2\nu)P_n}{2G_0} \\ 0 \end{pmatrix} \sin\left(\frac{1}{2}\beta_n(x+l)\right) \tag{8}$$

which holds for $-\infty < y < -y_c$. The most important quantity appearing within these expressions are the constants P_n, $n = 1, 2, ...$, defined as

$$P_n = -\frac{1}{l}\int_{-l}^{l} p(x)\sin\left(\frac{1}{2}\beta_n(x+l)\right)\mathrm{d}x \tag{9}$$

which are the coefficients in the Fourier series expansion of $p(x)$. These constants inform the dependence of the solution upon the applied pressure. The remaining quantities are defined in Appendix B.

As this paper considers lightly loaded contact between the indenter and solid, the applied pressure $P(x)$ in this problem will consist of only adhesive forces which are modelled using the Lennard Jones potential. In this situation, the contact pressure is assumed to be a function of the gap-width between the indenter and solid surface and is defined as follows [23, 25]

$$p(x) = -\frac{8\gamma}{3\epsilon}\left(\left(\frac{\epsilon}{h(x)}\right)^3 - \left(\frac{\epsilon}{h(x)}\right)^9\right) \tag{10}$$

where γ is the surface energy and h is the contact gap. The parameter ϵ is referred to as the atomic equilibrium spacing and represents the distance at which the total local intermolecular forces vanish. It is assumed that when $h(x) < \epsilon$, the indenter and solid surface will repel each other whilst when $h(x) > \epsilon$, the surfaces will attract each other. Finding the contact gap between surfaces is crucial if we are to use the Lennard Jones potential to model adhesive contact.

In the case of contact between a rigid cylindrical indenter and layered solid, we may formulate the following expression for the gap width

$$h(x) = -\alpha + \epsilon + \frac{x^2}{2R} + v(x,0), \tag{11}$$

where α is the approach of the indenter, $x^2/(2R)$ is the contact geometry and $v(x,0)$ is the surface deflection which may be computed from (6). We note that when $\alpha > 0$, the rigid indenter is being pressed into the layered solid.

In the work that follows, it is more convenient to work with a dimensionless pressure and gap-width rather than their dimensional counterparts.

Non-dimensionalising (10) and (11) using the transformations given in Appendix C yields the dimensionless quantities

$$p(X) = -\frac{8}{3}\left(\left(\frac{1}{H(X)+1}\right)^3 - \left(\frac{1}{H(X)+1}\right)^9\right), \tag{12}$$

$$\begin{aligned} H(X) &= -A + \frac{1}{2}X^2 + \frac{8\mu^{3/2}}{3\pi}v(X,0) \\ &= -\frac{8\mu^{3/2}}{3}\sum_{n=1}^{\infty}\xi_n^T(0)\Gamma_n\Omega_n\begin{pmatrix} \frac{(1-2\nu)P_n}{2G_0} \\ 0 \end{pmatrix}\sin\left(\frac{\sqrt{\epsilon R}\beta_n}{2}(X+L)\right) \\ &\quad -A + \frac{1}{2}X^2. \end{aligned} \tag{13}$$

Our aim within this work is to compute the gap-width for each value of X in $[-L, L]$ and hence determine the adhesive pressure acting on the solid. In order to do this, we compute the contact gap iteratively. Re-arranging (13) gives the residual term

$$\begin{aligned} R(X) &= \frac{8\mu^{3/2}}{3}\sum_{n=1}^{\infty}\xi_n^T(0)\Gamma_n\Omega_n\begin{pmatrix} \frac{(1-2\nu)P_n}{2G_0} \\ 0 \end{pmatrix}\sin\left(\frac{\sqrt{\epsilon R}\beta_n}{2}(X+L)\right) \\ &\quad +A - \frac{1}{2}X^2 + H(X). \end{aligned} \tag{14}$$

We note that $R(X)$ will be identically zero if the exact pressure is used to compute the Fourier coefficients P_n, whereas $R(X)$ will in general be non-zero if an approximation to the pressure is used instead. Minimising the residual term will ensure that an accurate approximation to $H(X)$ is returned. This idea forms the basis of the iterative algorithm described in figure 2. An initial approximation to $H(x)$ denoted $H_0(X)$ is used to calculate the pressure $p_0(X)$ and surface deflection $v_0(X,0)$. The residual term $R_0(X)$ is then computed and the algorithm proceeds by relaxing the computed surface deflection using the formulae

$$v_{i+1}(X,0) = v_i(X,0) - \delta R_i(X) \tag{15}$$

for $i = 0, 1, 2, ...$ until the the criterion

$$\max\left(R_i(X)\right) < 1 \times 10^{-6} \tag{16}$$

is met and the gap-width is deemed to be determined. The parameter δ is the relaxation factor and is allocated the value $\delta = 1 \times 10^{-2}$ within this work.

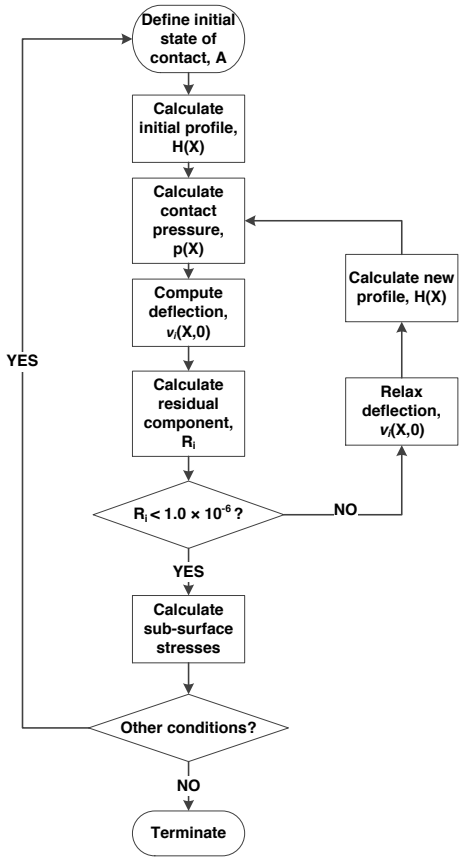

Figure 2: A flowchart of the iterative algorithm used to solve the adhesive contact problem.

In order to apply this algorithm, the interval $[-L, L]$ is discretised and split into M $(M > 2)$ sub-intervals. As a result, we obtain values of $H(X)$ and $p(X)$ only at a finite number of gridpoints and so the coefficients P_n cannot be computed using the formula given in (9) as this equation assumes a continuous pressure profile. The method used within this work to calculate

these quantities is detailed in Appendix D.

Solely determining the contact gap and applied pressure will not provide a complete picture of how the applied load propagates through the layered solid or how different coatings affect material response. Therefore, we also consider computing the sub-surface stress field, τ_1, within the layered solid which is computed from the formula

$$\tau_1 = \frac{1}{2}\sqrt{(\sigma_{xx}-\sigma_{yy})^2+4\sigma_{xy}^2}. \tag{17}$$

The stresses appearing in the formula above may be computed using Hooke's laws as

$$\begin{aligned}
\sigma_{xx} &= \frac{2G(y)}{(1-2\nu)}\left((1-\nu)\frac{\partial u}{\partial x}+\nu\frac{\partial v}{\partial y}\right),\\
\sigma_{yy} &= \frac{2G(y)}{(1-2\nu)}\left((1-\nu)\frac{\partial v}{\partial y}+\nu\frac{\partial u}{\partial x}\right),\\
\sigma_{xy} &= G(y)\left(\frac{\partial u}{\partial y}+\frac{\partial v}{\partial x}\right).
\end{aligned}$$

The partial derivatives of u and v may be easily evaluated from (5)-(8).

3. Results and Discussions

This study investigates lightly loaded contact during both the pre and initial contact region in an attempt to determine both the influence of surface adhesion and the physical characteristics of the graded coating on the material response under pressure. The effects of using different coating types is investigated by varying the ratio G_1/G_0. It should be noted that softer coatings correspond to $G_1/G_0 < 1$ whilst $G_1/G_0 > 1$ corresponds to harder coatings. The effects of surface adhesion are characterised using Tabor's parameter which is defined as

$$\mu = \left(\frac{R\gamma^2}{E^2\epsilon^3}\right)^{\frac{1}{3}}. \tag{18}$$

Tabor's parameter has been used extensively by other authors (e.g. Johnson and Greenwood [27]) and it is well documented that if $\mu \gg 1$, homogeneous materials experience JKR-like behaviour whilst if $\mu \ll 1$, homogeneous materials experience DMT-like behaviour. We therefore associate larger values of μ with increasingly compliant materials in the discussion contained within this section.

In figure 3, the load-displacement curves produced for different ratios of G_1/G_0 are plotted at different values of Tabor's parameter, μ, subject to the simulation parameters given in Appendix E. It can be observed within these plots that the harder coating ($G_1/G_0 = 2$) tends to generate a much higher negative force at different values of Tabor's parameter, μ.

Another distinct characteristic that can be identified in figure 3 is that when $\mu = 1$, discontinuities exist (at approximately 0.4nm) before the rigid indenter physically reaches the surface at $\alpha = 0$. This behaviour is known as the "snap-into" contact as a result of the attractive adhesive force pulling the rigid indenter down. Such discontinuous behaviour has been widely observed through experiments via apparatus such as the atomic force microscope (AFM) [32, 33, 34] and it clearly indicates the importance of understanding the effect of adhesion as it can cause premature contact. The adhering effect where the indenter and surface are being attracted to each other could induce large tensile stresses within the solid, possibly leading to yielding.

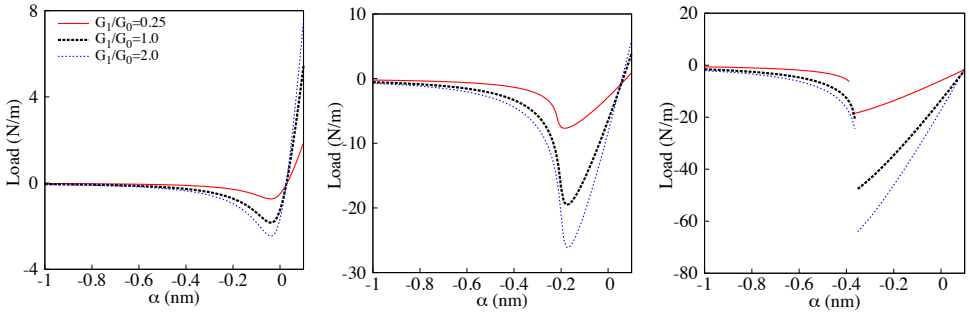

(a) $\mu = 0.1$ (b) $\mu = 0.5$ (c) $\mu = 1.0$

Figure 3: Load-Displacement curves (variation of G_1/G_0 with non-dimensional coating thickness, $Y_c = 0.5$)

The pressure distribution and surface vertical deflection of the investigated

contact are given in figure 4 at the contact state, $\alpha = 0$ subject to three different values of μ. It is observed that the predicted pressure increases dramatically as μ increases, with an order of magnitude difference between the pressures predicted when $\mu = 0.1$ and $\mu = 1$. We also observe that the contact involving the hard coating $G_1/G_0 = 2$ generates a much larger pressure than the soft coating $G_1/G_0 = 0.25$ but the surface deflection experienced by the soft coating is much larger. It should be noted here that as we consider only lightly loaded contacts, the solid surface will be in tension and thus surface deflection will be positive.

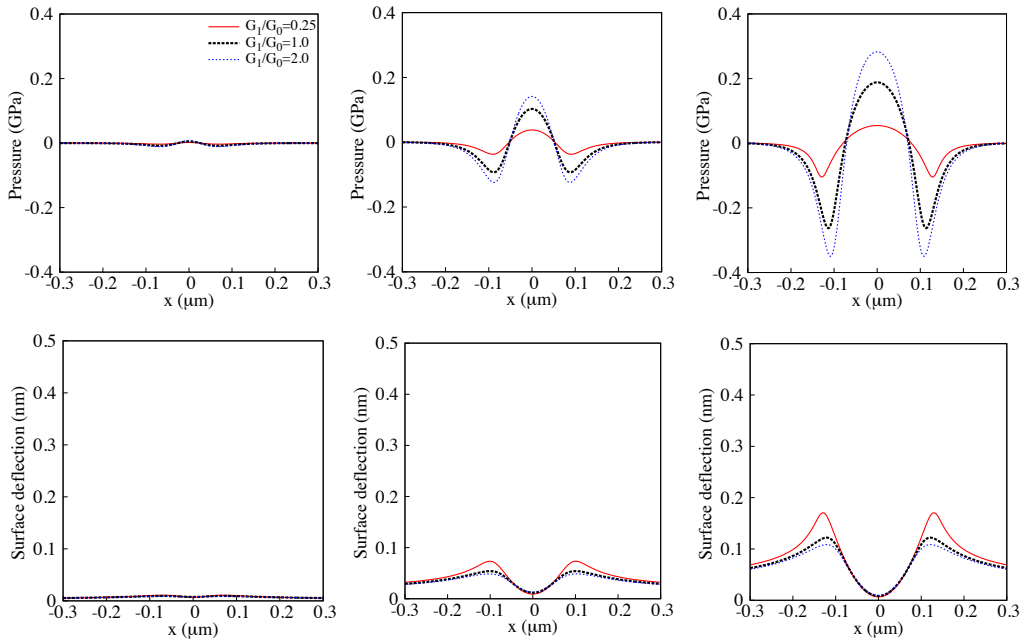

(a) $\mu = 0.1$ (b) $\mu = 0.5$ (c) $\mu = 1.0$

Figure 4: Contact pressure distribution and surface vertical deflection plots at $\alpha = 0$nm (variation of G_1/G_0 with non-dimensional coating thickness, $Y_c = 0.5$)

Figure 5 depicts the sub-surface stress fields corresponding to the pressure curves given in figure 4. It is easily seen here that the maximum stress within the solid increases as μ increases for all three values of G_1/G_0. We also observe here that subject to a fixed value of μ, the solid with the hard coating experiences a much larger maximum stress than the solid with the soft coating We note in particular that a region of high stress occurs close to the solid surface in the hard coating that begins to disperse sideways as

μ increases. This characteristic is also observed in the homogeneous solid but is absent within the soft coating. These results suggest that for highly sticky surfaces, layered solids comprising a hard coating are far more likely to experience plastic deformation than soft coatings. In such situations, an alternate model will need to be considered as the model proposed within this study will no longer apply.

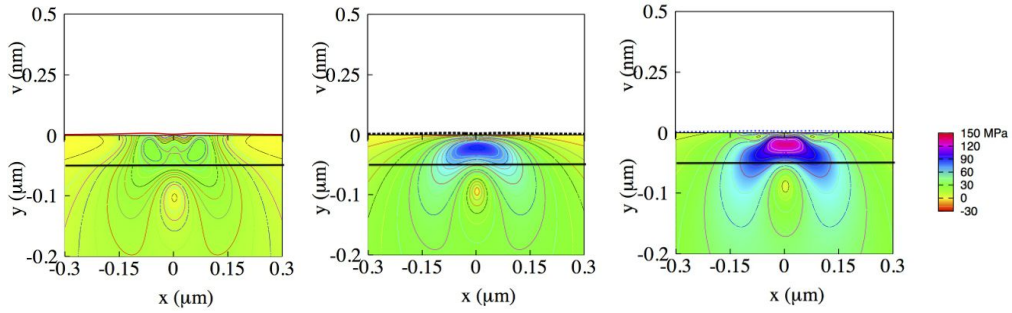

(a) $\mu = 0.1$, $G_1/G_0 = 0.25$ (b) $\mu = 0.1$, $G_1/G_0 = 1.001$ (c) $\mu = 0.1$, $G_1/G_0 = 2.00$

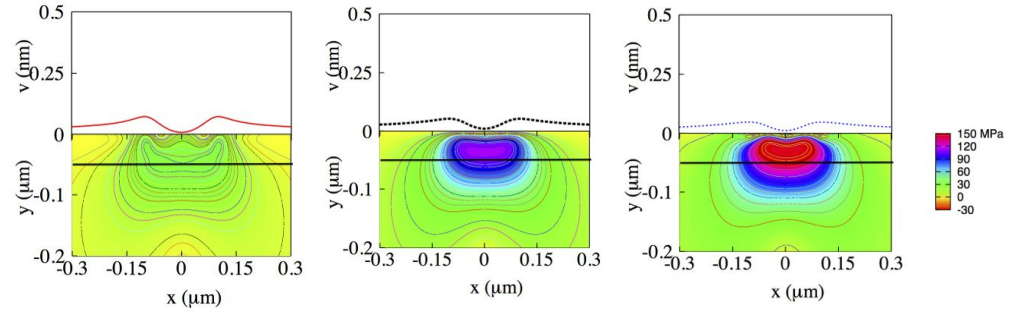

(d) $\mu = 0.5$, $G_1/G_0 = 0.25$ (e) $\mu = 0.5$, $G_1/G_0 = 1.001$ (f) $\mu = 0.5$, $G_1/G_0 = 2.00$

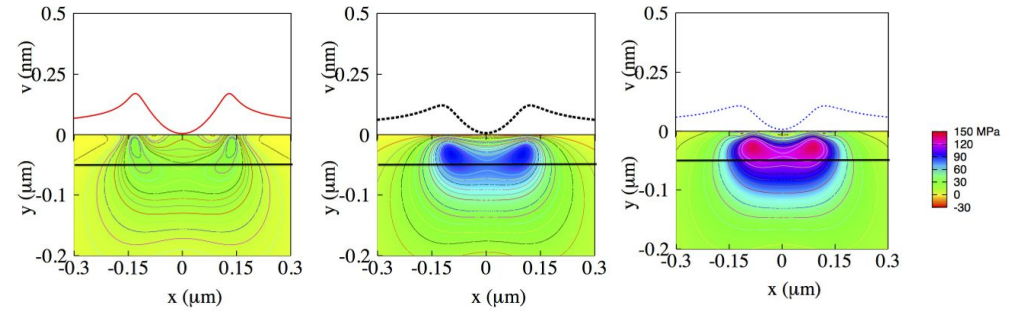

(g) $\mu = 1.0$, $G_1/G_0 = 0.25$ (h) $\mu = 1.0$, $G_1/G_0 = 1.001$ (i) $\mu = 1.0$, $G_1/G_0 = 2.00$

Figure 5: Subsurface stress fields at $\alpha = 0$nm (variation of G_1/G_0 with non-dimensional coating thickness, $Y_c = 0.5$)

Figure 6 illustrates the contact pressure distribution and surface deflection of the layered solid for three different coating types subject to the different values of α given. The generated pressure within the contact is initially

negative which shows a slight attraction between surfaces due to the surface energy. As the indenter gets closer to the solid surface and the gap decreases to $\alpha = -0.35$nm, the surface is pulled strongly towards the indenter, as indicated by the surface deflection curves. As the surfaces are moved closer together still, the repulsive characteristic along the contact tip region becomes apparent which eventually yields a positive pressure that contributes to the load carrying capacity of the contact.

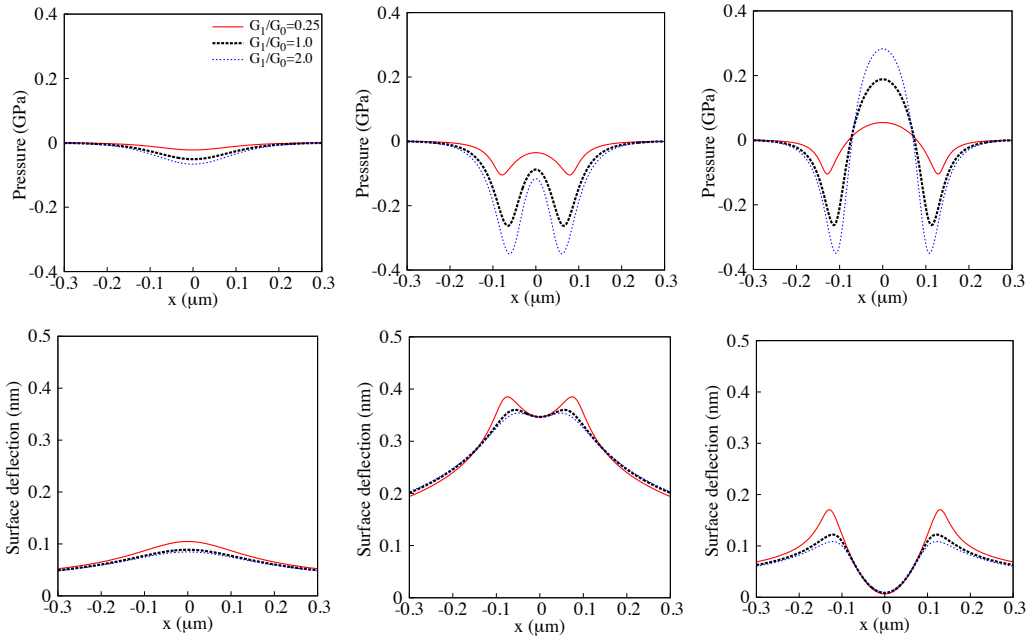

(a) $\alpha = -0.4$nm (b) $\alpha = -0.35$nm (c) $\alpha = 0$nm

Figure 6: Contact pressure distribution and surface vertical deflection plots at different α values (variation of G_1/G_0 with non-dimensional coating thickness, $Y_c = 0.5$ and Tabor's parameter, $\mu = 1$)

The sub-surface stress fields corresponding to the pressure profiles in figure (6 are presented in figure 7. A general trend that can be observed here is that the critically stressed region occurs along the edge of the contact region. This is a result of the surface adhesion attracting the surfaces and eventually pulling them together. We additionally note that the maximum principal stress for all three coating types increases in magnitude as the distance between surfaces decreases.

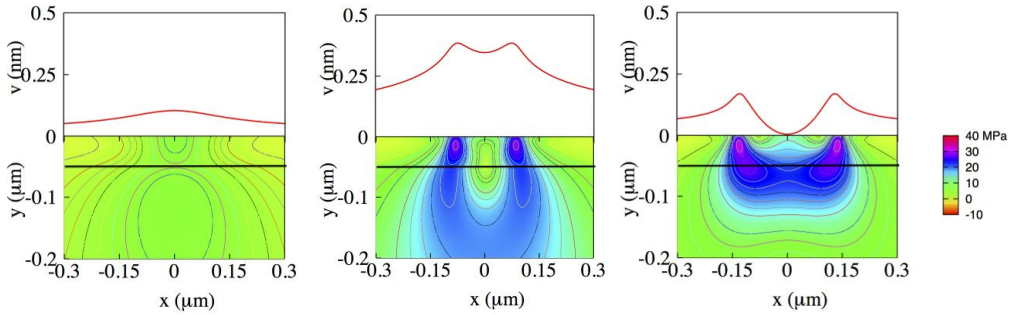

(a) $G_1/G_0 = 0.25$, $\alpha = -0.4$nm (b) $G_1/G_0 = 0.25$, $\alpha = -0.35$nm (c) $G_1/G_0 = 0.25$, $\alpha = 0$nm

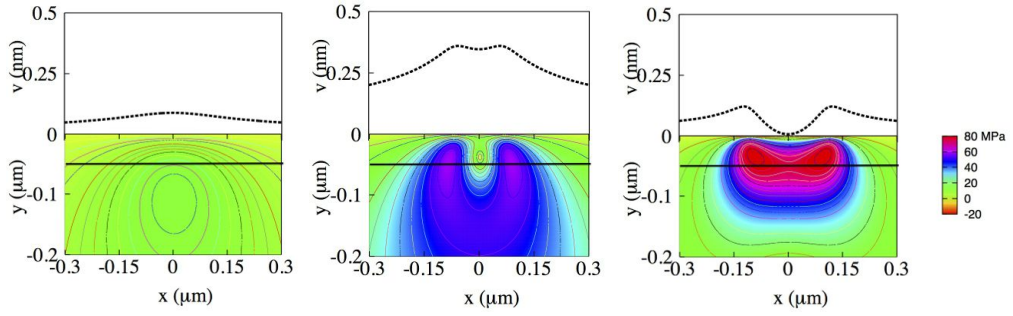

(d) $G_1/G_0 = 1.001$, $\alpha = -0.4$nm (e) $G_1/G_0 = 1.001$, $\alpha = -0.35$nm (f) $G_1/G_0 = 1.001$, $\alpha = 0$nm

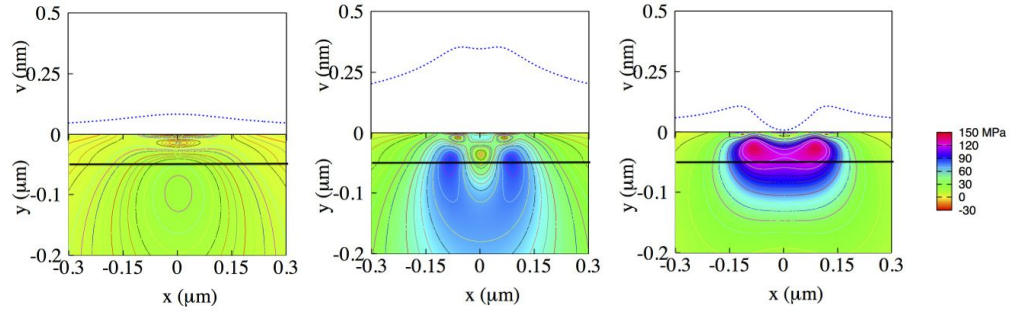

(g) $G_1/G_0 = 2.0$, $\alpha = -0.4$nm (h) $G_1/G_0 = 2.0$, $\alpha = -0.35$nm (i) $G_1/G_0 = 2.0$, $\alpha = 0$nm

Figure 7: Subsurface stress fields at different α values (variation of G_1/G_0 with non-dimensional coating thickness, $Y_c = 0.5$ and Tabor's parameter, $\mu = 1$)

The results discussed above have assumed a non-dimensional coating thickness of $Y_c = 0.5$. However the thickness of a particular coating could change the predicted material response significantly and so we conclude this study

with an investigation into the effects of coating thickness. Figure 8 depicts the load displacement curves, predicted pressure curves and surface deflection for both a hard and soft coating subject to three different coating thicknesses. We can see that the load-displacement curves presented show little variation with coating thickness. However, it is observed that an increase in coating thickness for a hard coating leads to an increase in the maximum pressure and a decrease in the maximum surface deflection. The converse is true for the soft coating as an increase in coating thickness here leads to an decrease in the applied maximum pressure and an increase in the maximum surface deflection. These trends are in accord with the observations of Chidlow *et al* [31].

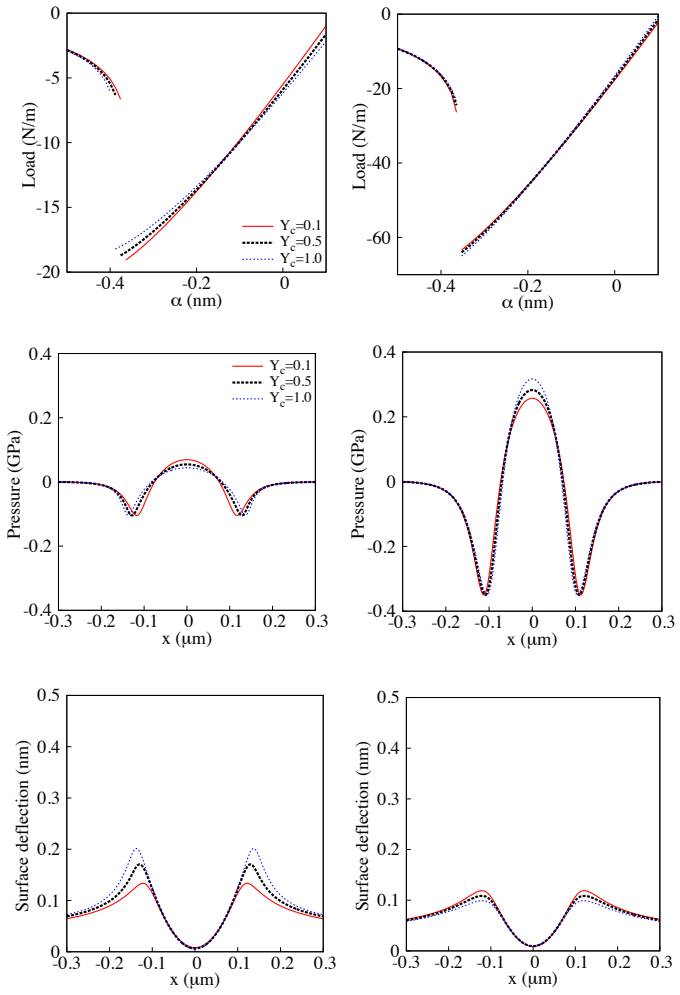

(a) $G_1/G_0 = 0.25$ (b) $G_1/G_0 = 2.0$

Figure 8: Contact pressure distribution and surface vertical deflection plots with different coating thickness, Y_c at $\alpha = 0$nm (variation of G_1/G_0 with Tabor's parameter, $\mu = 1$)

The sub-surface stress fields given in figure 9 correspond to the pressure curves presented in figures 8c and 8d. We can clearly see here that for both the hard and soft coating, the largest stress concentrations occur in the substrate for the thinnest coating ($Y_c = 0.1$). However, as the coating thickness increases, the regions of largest stress move into the coating. This is potentially significant in determining the onset of plastic yielding as small changes in the thickness of a hard coating can lead to much larger maximum

stresses as indicated in figures 9c and 9f.

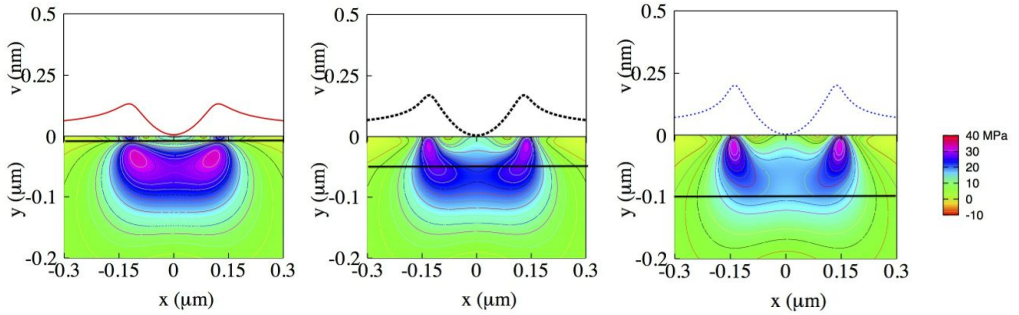

(a) $Y_c = 0.1$, $G_1/G_0 = 0.25$ (b) $Y_c = 0.5$, $G_1/G_0 = 0.25$ (c) $Y_c = 1.0$, $G_1/G_0 = 0.25$

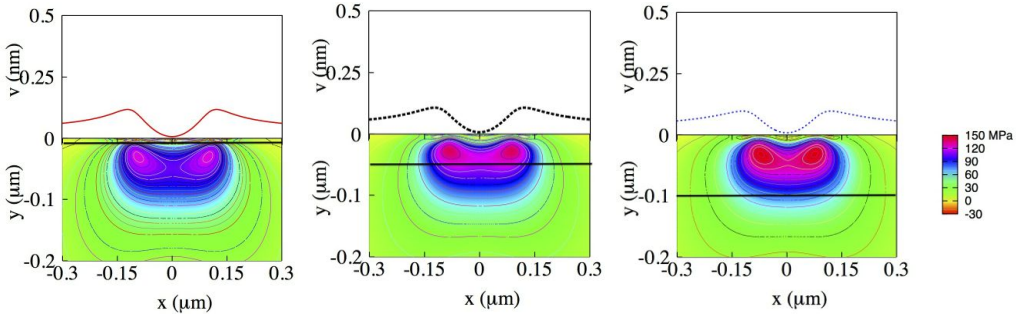

(d) $Y_c = 0.1$, $G_1/G_0 = 2.0$ (e) $Y_c = 0.5$, $G_1/G_0 = 2.0$ (f) $Y_c = 1.0$, $G_1/G_0 = 2.0$

Figure 9: Subsurface stress fields with different coating thickness, Y_c at $\alpha = 0$nm (variation of G_1/G_0 with Tabor's parameter, $\mu = 1$)

4. Conclusion

This study has been concerned with the effects of adhesion in the contact problem involving a rigid cylinder and layered elastic solid comprising a functionally graded coating perfectly bonded to a homogenous substrate under lightly loaded conditions. The surface adhesive force was modelled using the Lennard-Jones potential and the behaviour of the solid is determined using the model of Chidlow *et al* [10]. The investigation concentrated primarily on determining the effects of the variation in the shear modulus G_1/G_0, Tabor's parameter, μ and the coating thickness, y_c on the predicted pressure, surface deflection and sub-surface stress fields induced within the pre and initial contact region.

The numerical results presented have shown that contact can occur before the surfaces physically touch each other at $\alpha = 0$ because of the attractive adhesive forces present. This work also demonstrated that there is a need to understand the effects of surface adhesion at a small scale when designing coatings of a functionally graded nature, at pre and initial contact. This is because when the contact is repeatedly loaded and unloaded, a region of high stress is observed to occur along the edges of the contact which could initiate plastic flow and adhesive wear as a result of fatigue yielding and lead to the exfoliation of protective coatings. The work within this study further provides an opportunity to investigate adhesive wear for sliding contact problems.

Acknowledgement

The authors acknowledge the technical support from partners and sponsorship provided by the EPSRC through the ENCYCLOPAEDIC program grant.

References

[1] S. Suresh. Graded materials for resistance to contact deformation and damage. *Science*, 292(5526):2447–2451, 2001.

[2] Tohru Hirano and Kenji Wakashima. Mathematical modeling and design. *MRS Bull*, 20(01):40–42, 1995.

[3] F. Erdogan, A. C. Kaya, and P. F. Joseph. The mode iii crack problem in bonded materials with a nonhomogeneous interfacial zone. *J. App. Mech.*, 58(2):419–427, 1991.

[4] H. Hertz. On the contact of elastic solids. *J. reine angew. Math*, 92(156-171):110, 1881.

[5] A. E. Giannakopoulos and S. Suresh. Indentation of solids with gradients in elastic properties: Part i. point force. *Int. J. Solids and Struct.*, 34(19):2357–2392, 1997.

[6] Z. Wang, H. Wang, W.and Wang, D. Zhu, and Y. Hu. Partial slip contact analysis on three-dimensional elastic layered half space. *J. Trib.*, 132(2):021403, 2010.

[7] M. A. Guler and F. Erdogan. Contact mechanics of graded coatings. *Int. J. Solids and Struct.*, 41(14):3865–3889, 2004.

[8] L. Ke and Y. Wang. Two-dimensional sliding frictional contact of functionally graded materials. *Eur. J. Mech. A/solids*, 26(1):171–188, 2007.

[9] M. Teodorescu and H. Rahnejat. Mathematical modelling of layered contact mechanics of cam tappet conjunction. *App. Math. Modell.*, 31:2610–2627, 2007.

[10] S. J. Chidlow, M. Teodorescu, and N. D. Vaughan. Predicting the deflection and sub-surface stress field within two dimensional in homogeneously elastic bonded layered solids under pressure. *Int. J. Solids and Struct.*, 48:3243–3256, 2011.

[11] W. W. F. Chong. A numerical model for wet-adhesive line contact. *Proc. Eng.*, 68:579–585, 2013.

[12] W. W. F. Chong, M. Teodorescu, and H. Rahnejat. Nanoscale elastoplastic adhesion of wet asperities. *Proc. IMechE: Part J: J. Eng. Trib.*, 227:996–1010, 2013.

[13] J. Boussinesq. *Application des potentiels à l'étude de l'équilibre et du mouvement des solides élastiques: principalement au calcul des déformations et des pressions que produisent, dans ces solides, des efforts quelconques exercés sur une petite partie de leur surface ou de leur intérieur. Mémoire suivi de notes étendues sur divers points de physique mathématique et d'analyse..* A. Blanchard, 1969.

[14] R. S. Bradley. The cohesive force between solid surfaces and the surface energy of solids. *The London, Edinburgh, and Dublin Philosophical Magazine and Journal of Science*, 13(86):853–862, 1932.

[15] H. C. Hamaker. The london?van der waals attraction between spherical particles. *physica*, 4(10):1058–1072, 1937.

[16] B. V. Derjaguin. Untersuchungen über die reibung und adhäsion, iv. *Colloid & Poly. Sci.*, 69(2):155–164, 1934.

[17] K. L. Johnson, K. Kendall, and A. D. Roberts. Resolving the contradiction of asperities plastic to elastic mode transition in current contact

models of fractal rough surfaces. *Proc. Roy. Soc., Series A*, 324:301–313, 1971.

[18] B. V. Derjaguin, V. M. Muller, and Y. P. Toporov. Effect of contact deformation on the adhesion of elastic solids. *J. Colloid and Interface Sci.*, 53:314–326, 1975.

[19] D. S. Grierson, E. E. Flater, and R. W. Carpick. Accounting for the jkr-dmt transition in adhesion and friction measurements with atomic force microscopy. *J. Adh. Sci. and Tech.*, 19(3-5):291–312, 2005.

[20] D. Tabor. Surface forces and surface interactions. *J. Colloid and Inter. Sci.*, 58(1):2–13, 1977.

[21] V. M. Muller, V. S. Yushchenko, and B. V. Derjaguin. On the influence of molecular forces on the deformation of an elastic sphere and its sticking to a rigid plane. *J. Colloid and Inter. Sci.*, 77(1):91–101, 1980.

[22] D. Maugis. On the contact and adhesion of rough surfaces. *J. Adhesion Sci. & Tech.*, 10:161–175, 1996.

[23] J. Q. Feng. Contact behavior of spherical elastic particles: a computational study of particle adhesion and deformations. *Colloids Surf. A*, 172:175–198, 2000.

[24] P Attard and J. L. Parker. Deformation and adhesion of elastic bodies in contact. *Phy. Rev. A*, 46(12):7959, 1992.

[25] J. J. Wu. Adhesive contact between a cylinder and a half-space. *J. Phys. D: Appl. Phys*, 42:155302, 2009.

[26] Y. S. Leng, Y. Z. Hu, and L. Q. Zheng. Adhesion of smoothly flat–ended wedges. *Proc. Roy. Soc, Lon.. Ser. A: Math., Phy. and Eng. Sci.*, 456(1993):185–204, 2000.

[27] K. L. Johnson and J. A. Greenwood. A maugis analysis of adhesive line contact. *J. Phy. D: App. Phy.*, 41(15):155315, 2008.

[28] P. M. McGuiggan, J. S. Wallace, D. T. Smith, I. Sridhar, Z. W. Zheng, and K. L. Johnson. Contact mechanics of layered elastic materials: experiment and theory. *J. Phy. D: App. Phy.*, 40(19):5984, 2007.

[29] P. Mary, A. Chateauminois, and C. Fretigny. Deformation of elastic coatings in adhesive contacts with spherical probes. *J. Phy. D: App. Phy.*, 39(16):3665, 2006.

[30] K. L. Johnson and I. Sridhar. Adhesion between a spherical indenter and an elastic solid with a compliant elastic coating. *J. Phy. D: App. Phy.*, 34(5):683, 2001.

[31] S. J. Chidlow, W. W. F. Chong, and M. Teodorescu. On the two dimensional solution of both adhesive and non-adhesive contact problems involving functionally graded materials. *Eur. J. Mech. A/solids*, 39:86–103, 2013.

[32] L. Heim, J. Blum, M. Preuss, and H. Butt. Adhesion and friction forces between spherical micrometer-sized particles. *Phys. Rev. Letts.*, 83(16):3328, 1999.

[33] E. R. Beach, G. W. Tormoen, J. Drelich, and R. Han. Pull-off force measurements between rough surfaces by atomic force microscopy. *J. Colloid and Interface Sci.*, 247(1):84–99, 2002.

[34] G. Huber, S. N. Gorb, R. Spolenak, and E. Arzt. Resolving the nanoscale adhesion of individual gecko spatulae by atomic force microscopy. *Bio. Letts.*, 1(1):2–4, 2005.

Appendix A. Nomenclature

A	Non-dimensional initial state of contact $(-)$
E_0	Young's modulus of the substrate (Pa)
E_1	Young's modulus on the surface of the coating(Pa)
G_0	Shear modulus of the substrate (Pa)
G_1	Shear modulus on the surface of thesubstrate (Pa)
G	Shear modulus of the functionally graded coating (Pa)
H	Non-dimensional contact gap $(-)$
L	Non-dimensional contact width $(-)$
P	Non-dimensional contact pressure $(-)$
R	Indenter curvature radius (m)
R_i	Residual term $(-)$
U	Non-dimensional deflection in x-direction $(-)$
V	Non-dimensional deflection in y-direction $(-)$

X	Non-dimensional horizontal co-ordinate $(-)$
Y	Non-dimensional vertical co-ordinate $(-)$
h	Contact gap (m)
p	Contact pressure (Pa)
u	Deflection in x-direction (m)
v	Deflection in y-direction (m)
x	Horizontal co-ordinate (m)
y	Vertical co-ordinate (m)
Ω	Relaxation term $(-)$
α	Approach of indenter (m)
l	Contact width (m)
ϵ	Atomic equilibrium spacing (m)
μ	Tabor's parameter $(-)$
ν	Poisson's ratio of the solid $(-)$
σ_{yy}	Normal stress in the y-direction (Pa)
σ_{xx}	Normal stress in the x-direction (Pa)
σ_{xy}	Shear stress (Pa)
τ_1	Principal stress (Pa)

Appendix B. List of quantities appearing in the contact model

This section provides a list of all of the quantities appearing in the model derived by Chidlow *et al.* [31] except for the Fourier coefficients defined in (9).

CONSTANTS:

$$
\begin{aligned}
\rho &= \frac{\nu}{1-\nu}, \\
\beta_n &= \frac{n\pi}{l}, \\
\delta_n &= \frac{2(3-4\nu)}{\beta_n}, \\
\lambda_{1,n} &= \sqrt{\frac{1}{4}(\zeta^2+\beta_n^2)+\frac{i}{2}\zeta\beta_n\sqrt{\rho}}-\frac{1}{2}\zeta, \\
\lambda_{2,n} &= -\sqrt{\frac{1}{4}(\zeta^2+\beta_n^2)+\frac{i}{2}\zeta\beta_n\sqrt{\rho}}-\frac{1}{2}\zeta, \\
\lambda_{3,n} &= \sqrt{\frac{1}{4}(\zeta^2+\beta_n^2)-\frac{i}{2}\zeta\beta_n\sqrt{\rho}}-\frac{1}{2}\zeta, \\
\lambda_{4,n} &= -\sqrt{\frac{1}{4}(\zeta^2+\beta_n^2)-\frac{i}{2}\zeta\beta_n\sqrt{\rho}}-\frac{1}{2}\zeta, \\
\gamma_{j.n} &= \frac{2\left((1-2\nu)\lambda_{j,n}^2+\zeta(1-2\nu)\lambda_{j,n}-\frac{1}{2}(1-\nu)\beta_n^2\right)}{\beta_n(\lambda_{j,n}+\zeta(1-2\nu))}, \\
\tau_{j,n} &= 1+\gamma_{j,n},
\end{aligned}
$$

where $j = 1, 2$, $n = 1, 2, ..., N$.

MATRICES:

The following matrices are all size 2×2.

$$
\begin{aligned}
W_n &= N_{1,n} - N_{2,n}\left(T_{2,n}\mathcal{K}_{2,n}\right)^{-1} T_{1,n}\mathcal{K}_{1,n}, \\
\Psi_n &= \left(Z_{1,n} - Z_{2,n}T_{2,n}^{-1}T_{1,n}\right)\mathcal{K}_{1,n}W_n^{-1}, \\
\Phi_n &= \begin{pmatrix} 1 & -\delta_n \\ 0 & 1 \end{pmatrix}, \\
\mathcal{K}_{j,n} &= \operatorname{diag}(e^{-\lambda_{j,n}y_c}, e^{-\lambda_{j+2,n}y_c}), \\
T_{j,n} &= N_{j,n} + \frac{1}{\delta_n}M_{j,n}, \\
Z_{j.n} &= \begin{pmatrix} \delta_n + y_c\tau_{j,n} & \delta_n + y_c\tau_{j+2,n} \\ \tau_{j,n} & \tau_{j+2,n} \end{pmatrix}, \\
M_{j,n} &= \begin{pmatrix} \frac{1}{2}(1-2\nu)\left(4(1-\nu)\tau_{j,n} - \beta_n\delta_n\right) & \frac{1}{2}(1-2\nu)\left(4(1-\nu)\tau_{j+2,n} - \beta_n\delta_n\right) \\ 2(1-2\nu)(1+\gamma_{j,n}) - \beta_n\delta_n & 2(1-2\nu)(1+\gamma_{j+2,n}) - \beta_n\delta_n \end{pmatrix}, \\
N_{j,n} &= \begin{pmatrix} -\left(\frac{1}{2}\nu\beta_n + (1-\nu)\lambda_{j,n}\gamma_{j,n}\right) & -\left(\frac{1}{2}\nu\beta_n + (1-\nu)\lambda_{j+2,n}\gamma_{j+2,n}\right) \\ \lambda_{j,n} - \frac{1}{2}\beta_n\gamma_{j,n} & \lambda_{j+2,n} - \frac{1}{2}\beta_n\gamma_{j+2,n} \end{pmatrix}.
\end{aligned}
$$

The matrices given below are size 4×2.

$$
\begin{aligned}
\Gamma_n &= \operatorname{diag}\left(\gamma_{1,n}, \gamma_{3,n}, \gamma_{2,n}, \gamma_{4,n}\right), \\
\Omega_n &= \begin{pmatrix} W_n^{-1} \\ \left(T_{2,n}\mathcal{K}_{2,n}\right)^{-1}T_{1,n}\mathcal{K}_{1,n}W_n^{-1}. \end{pmatrix}
\end{aligned}
$$

Note in all quantities given above that $j = 1, 2$ and $n = 1, 2, ..., N$.

VECTORS:

$$
\begin{aligned}
\xi_n(y) &= \left(e^{\lambda_{1,n}y}, e^{\lambda_{2,n}y}, e^{\lambda_{3,n}y}, e^{\lambda_{4,n}y}\right)^T, \\
\varphi(y) &= (1, y)^T
\end{aligned}
$$

where $n = 1, 2, ..., N$.

Appendix C. List of the non-dimensionalisations used within this work

$$\begin{aligned} H &= h/\epsilon - 1 \\ A &= \alpha/\epsilon \\ V &= v/\epsilon \\ X &= x/\sqrt{\epsilon R} \\ Y &= Y/\sqrt{\epsilon R} \\ L &= \ell/\sqrt{\epsilon R} \\ \mu &= [R\gamma^2/(E^2\epsilon^3)]^{1/3} \\ \frac{1}{E} &= \frac{1-\nu_0^2}{E_0} + \frac{1-\nu_1^2}{E_1} \end{aligned}$$

Appendix D. Computing Fourier Coefficients given a discrete pressure function

The Fourier coefficients appearing within the model may be computed from the dimensionless pressure using the formula

$$P_n = -\frac{\sqrt{\epsilon R}}{L}\int_{-L}^{L} p(X)\sin\left(\frac{\sqrt{\epsilon R}\beta_n}{2}(X+L)\right)\mathrm{d}X, \tag{D.1}$$

where $n = 1, 2, ...$ As the pressure obtained in this problem will be known at only a finite number of values of X however, we must make the applied pressure continuous by fitting a linear spline. Assuming that the interval $-L \leq X \leq L$ is sub-divided into M sub-intervals where $M > 2$, this returns the approximation

$$p(X) \approx \sum_{j=1}^{M+1} P_j \phi_j(X) \tag{D.2}$$

where

$$\phi_j(X) = \begin{cases} \frac{X - X_{j-1}}{X_j - X_{j-1}}, & X_{j-1} \leq X \leq X_j, \\ \frac{X_{j+1} - X}{X_{j+1} - X_j}, & X_j \leq X \leq X_{j+1} \end{cases} \tag{D.3}$$

for $j = 2, ..., M$ and P_j is the approximation to the dimensionless pressure at the jth gridpoint. The remaining functions appearing above are defined as

$$\phi_1(X) = \frac{X_2 - X}{X_2 - X_1}, \qquad X_1 \leq X \leq X_2, \tag{D.4}$$

$$\phi_{M+1}(X) = \frac{X - X_M}{X_{M+1} - X_M}, \qquad X_M \leq X \leq X_{M+1}. \tag{D.5}$$

Substituting (D.2) into (D.1) returns the approximation

$$P_n = -\frac{1}{L} \sum_{j=1}^{M+1} P_j \int_{-L}^{L} \phi_j(X) \sin\left(\frac{\sqrt{\epsilon R}\beta_n}{2}(X + L)\right) \mathrm{d}X, \tag{D.6}$$

for $n = 1, 2, ...$

Appendix E. Simulation Parameters

	Parameters	**Values**	**Units**
1.	R	40	μm
2.	ϵ	0.235	nm
3.	E_0	200	GPa
4.	ν	0.23	-

We note that the infinite summations appearing in (5)-(8) are truncated to contain 300 terms within this investigation.